REGULAR ARTICLE

Incorporating 2D tree-ring data in 3D laser scans of coarse-root systems

Bettina Wagner · Holger Gärtner · Hilmar Ingensand · Silvia Santini

Abstract In times of global change biomass calculations and the carbon cycle is gaining in importance. Forests act as carbon sinks and hence, play a crucial role in worlds and forests carbon budgets. Unfortunately, growth models and biomass calculations existing so far mainly concentrate on the above-ground part of trees. For this reason, the aim of the present study is to develop an annually resolved 3D growth model for tree roots, which allows for reliable biomass calculations and can later be combined with above-ground models. A FARO scan arm was used to measure the surface of a tree-root segment. In addition, ring-width measurements were performed manually on sampled cross sections using Win-DENDRO. The main goal of this study is to model root growth on an annual scale by combining these data sets. In particular, a laser scan arm was tested as a device for the realistic reproduction of tree-root architecture, although the first evaluation has been performed for a root segment rather than for an entire root system. Deviations in volume calculations differed between 5% and 7% from the actual volume and varied depending on the used modeling technique. The model with the smallest deviations represented the structure of the root segment in a realistic way and distances and diameter of cross sections were acceptable approximations of the real values. However, the volume calculations varied depending on object complexity, modeling technique and order of modeling steps. In addition, it was possible to merge tree-ring borders as coordinates into the surface model and receive age information in connection with the spatial allocation. The scan arm was evaluated as an innovative and applicable device with high potential for root modeling. Nevertheless, there are still many problems connected with the scanning technique which have an influence on the accuracy of the model but are expected to improve with technical progress.

Keywords Laser scanning · Tree roots · Root modeling · Biomass · Tree rings

Responsible Editor: Alexia Stokes.

B. Wagner (✉) · H. Gärtner
Swiss Federal Research Institute WSL,
Zürcherstrasse 111,
8903 Birmensdorf, Switzerland
e-mail: bettina.wagner@wsl.ch

B. Wagner · H. Ingensand
Institute of Geodesy and Photogrammetry, ETH Zurich,
8093 Zurich, Switzerland

S. Santini
Institute for Pervasive Computing, ETH Zurich,
8092 Zurich, Switzerland

Introduction

Forests contribute with 30% to Earth's land surface (Brunner and Godbold 2007) and, hence, forest

 Springer

biomass plays a crucial role in the global carbon cycle (Cheng et al. 2007). 20–40% of total forest biomass is accounted for by roots (Brunner and Godbold 2007) depending on ecological conditions and tree species (Le Goff and Ottorini 2001). Therefore, to accomplish an overall biomass prediction for entire trees, forest stands, and local and global carbon budgets, root biomass calculations are crucial (Nielsen and Hansen 2006), and more precise calculations are needed (Gärtner and Bräker 2004). Moreover, detailed analyses regarding the annual development of root systems would be an important task in tree-ring research and for biomechanical studies. Whilst measurements of various parameters in tree stems as annual ring-width and anatomical variations are approved methods to analyze past environmental conditions, the influence of root systems on the development of these stems—or vise versa—has widely been neglected so far (Gärtner et al. 2009). In this regard, research concentrates on growth variations of single roots for detailed environmental reconstructions on a local scale (Gärtner et al. 2001; Gärtner 2007) but is rarely related to the stem development (Krause and Morin 1999; Drexhage et al. 1999). Although these measurements could be realized for samples of all single roots of a system, there is no possibility to reconstruct their exact position within the system for further comprehensive analyses. For doing so, precise models of the entire root system would be needed.

Root systems can be modeled considering different basic principles, at different scales and levels of detail. Studies usually concentrate either on geometry, topology, or biomass estimations (Danjon and Reubens 2008). Most models applied for biomass calculations are either bound to certain species and management methods or they rely on stand specific estimations (Bolte et al. 2004; Le Goff and Ottorini 2001; Nielsen and Hansen 2006). For these modeling approaches, the root systems have to be exposed to capture and analyze their volume and 3D structure. Hruska et al. (1999) suggested using ground penetrating radar for monitoring root development of unexposed root systems. However, later investigations demonstrated that the resolution of this technique and the special requirements (e.g., homogeneous, dry soils) are not sufficient to obtain a detailed picture of a root systems development (Stokes et al. 2002). Consequently, the exposure of the entire root system is still essential for further analysis.

The use of a 3D-digitizer was successfully applied to capture the geometry and topology of the roots to acquire the architecture of exposed root systems (Danjon et al. 1999, 2005). In this regard, a point-by-point exploration facilitates the measuring of the length of single roots and branching in three-dimensional space (Sinoquet and Rivet 1997). However, when it comes to volume quantifications models based on digitizing are due to cylindrical or cone-shaped root representations simplified approximations and do not represent the surface structure in a realistic way. Therefore, 3D models of root systems based on high resolution laser-scanning data provide additional and more comprehensive information about root architecture (e.g., branching patterns as a base to analyze tree anchorage) and, moreover, will shed light on biomass developments as well as on spatial patterns of the single roots. Furthermore, additional knowledge about ecosystem processes will be produced by including ring-width data and correlating the combined data to developmental stages of the stem (Gärtner et al. 2009).

A cost effective and time efficient way to capture the 3D structure of complex structures such as root systems is laser scanning (LS). The laser scanning technique has been established in geodesy, architecture, archaeology, and engineering science in the last decade and is frequently used in forestry. In this context, airborne (Lim et al. 2003; Rossmann and Bücken 2008) and terrestrial laser scanning (TLS) was applied to analyze, e.g., the canopy structure and stem density in order to describe the current state of a forest stand as a base for management activities (Aschoff and Spiecker 2004; Maas et al. 2008; Pfeifer and Winterhalder 2004; Teobaldelli et al. 2008). In this context, below-ground structures have been mainly neglected except for two applications where entire root systems were scanned using TLS systems (Gärtner and Denier 2006; Gärtner et al. 2009; Teobaldelli et al. 2007). More advanced systems are scan arms which, in contrast to TLS, are not fixed to a static position and thus have an optimum range for scanning on short distances (up to 60 mm). Scan arms reach higher accuracy and are supposed to reach even better results in terms of volume computations than TLS. According to Danjon and Reubens (2008) laser scanning is stated to be the best available technique to describe the surface and shape of roots existing so far. However, the resulting model displays the time of

uprooting and is thus unable to give additional information regarding the spatio-temporal development of the root system. On the other hand, understanding anchorage, developmental processes, and possible shifts in carbon storage between above and below-ground parts of the trees, would represent a significant step towards the development of a model showing the annual development of a root system.

A project was started at the Swiss Federal Research Institute WSL to develop a new methodology for modeling of coarse root systems down to a size of 0.5 cm of single roots. To realize this, three main steps are required: (1) capturing the 3D structure (architecture) of the entire root system in high resolution, (2) measuring the annual development (ring-width measurements) of single root segments, and (3) combining these data layers into a single, annually resolved spatio-temporal model of the entire root system. The successful application of such a new method will for the first time provide fundamental data for quantifying the below-ground biomass and the annually resolved interrelation between above- and below-ground productivity. In addition, branching patterns and root length can be retraced and analyzed within the model.

The study presented in this paper, concentrates on the fundamental challenge of the above mentioned project, namely on the development of an effective way to integrate 2D ring-width data into the 3D model of a root segment, which was captured by the first time application of a scan arm. The successful integration of ring-width data to such a model is a basic requirement for all further analyses of root system development.

Material and methods

Laser scanning technique

A Faro Platinum Scan Arm (FARO 2009) with a reverse measuring principle was used to acquire the 3D structure of a root segment. The scanner device itself is attached to an articulated arm with seven axis and spherical working volumes, i.e. 3 translational joints (circles with arrows in Fig. 1) are combined with 4 rotational joints (360°) to enable a free orientation of the scanning device mounted at the end of the arm. The operator directs the scan device interactively along the surface of the scan object.

Within each joint rotary encoders are integrated, who's signals are processed and positional data are sent to a connected computer (FARO 2009).

For this study, the scan device was equipped with a FARO laser line probe projecting the laser beam as a line on the surface of any object (Fig. 1, Table 1). While emitting the beam line, an integrated camera takes a picture of the shape and the exact position of the line on the surface of the scanned object and registers x/y/z-coordinates along the line (FARO 2009). Due to the calibrated and known length of the segments and the highly precise goniometers the position of the probes and laser scanner can be determined (Merk 2007).

Before starting the scanning procedure, various parameters influencing the scan procedure need to be considered because they can possibly cause instrumental and non-instrumental measurement errors occurring due to the experimental setup or because of the properties of the scanned object (Schulz 2007). Concerning the main non-instrumental errors the intensity of the laser beam and the surface properties of the scanned object need to be taken into account (Schulz and Ingensand 2004). These errors are mainly related to the distance between the scanner and the object, because the amplitude of the received signal influences the quality of the detecting range (Lichti et al. 2005). Additionally, the angle in which the beam tangents the surface of an object (angle of incidence) influences the footprints of the beam on the surfaces. Due to these deformations the point of reference might not be well-defined and thus, distances might deviate from reality. Therefore, simple shapes like cylinders and objects of wood, metal and paper with different surface characteristics (roughness, color, and reflectance) were scanned, to quantify and eliminate these possible errors. This was also done to become aware of the test sensitivity related to different factors as scattering- and shadowing effects (Lichti et al. 2005). Roots with a diameter less than 0.5 cm are removed to avoid unnecessary hinders for the scanning procedure. The roots are stored at room temperature before scanning them.

Due to obstacles and line-of-sight obstructions, it is impossible to acquire the entire surface of a 3D object from one scan direction (Schulz 2007). By using the Faro arm, the object can be scanned from different perspectives while the scanner software directly arranges the single scans in the correct orientation.

Fig. 1 Schematic view of the scanning procedure. The scanning device is attached to an articulated arm with 3 translational joints (*arrows*) which are combined with 4 rotational joints (360°). The laser probe is emitting a beam line to the object capturing the data for surface representation
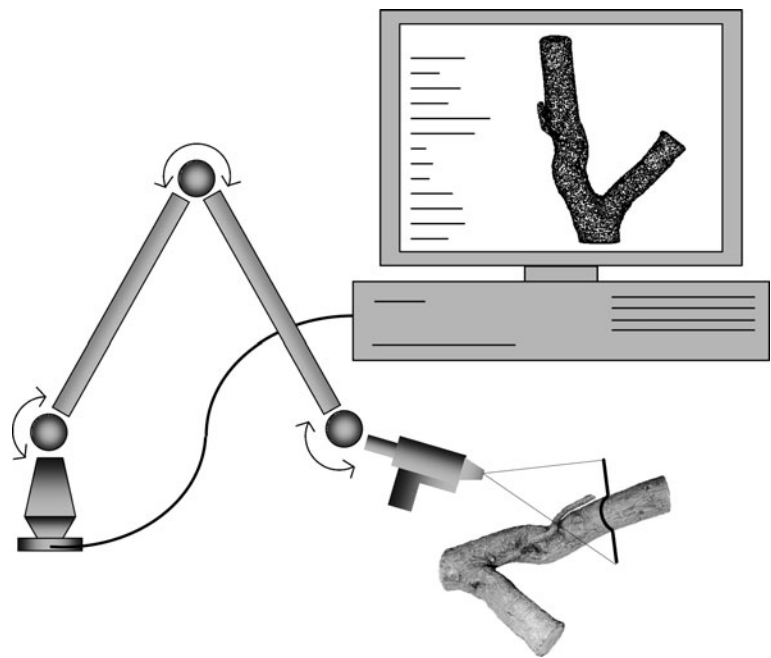
For huge root systems with complex branching structures it might be difficult to reach some of the hidden parts and the scan arm has to be moved and single scans manually registered.

Data processing

The possible detection errors discussed before may cause false data points or outliers in the point clouds (Schulz 2007). These outliers need to be removed from data sets because they can cause serious problems during modeling (Sotodeh 2006). This is done by applying filter functions and modeling techniques offered by Geomagic software to automatically reduce noise (Geomagic 2007). The influence of these techniques on the resulting model was examined by calculating deviations in volume com-

pared to a model with conservative filters. In any case, filter techniques are indispensable since without them no volume computation would be possible (Wagner and Gärtner 2009a). For a basic test of the accuracy of the model, water replacement tests were done. The deviation of the calculated to the real volume of the scanned simple objects was below 2%. However, there is an explicit difference in the amount of deviation depending on the particular shape of the scanned object. With increasing complexity of the scanned structures the deviation is increasing (deviations 5–7%) (Gärtner et al. 2009; Wagner and Gärtner 2009b). Bark can be particularly rough and has an impact on the scattering of data points. Especially when trying to generate a closed surface the roughness of the bark can have an impact on the meshing procedure. Due to outlier detection and additional

Table 1 Accuracy of point and line measurements using the Faro Platinum Scan Arm and the laser line probe

Accuracy single point measurement	50 μm
Accuracy of points for line measurement	± 68 μm (distance 1.2 m)
	± 76 μm (distance 1.8 m)
Effective scan width (length of line):	
Near field	34 mm
Far field	60 mm
Points per line:	640
Scan rate:	30 Lines / second × 640 Points / Line = 19200 Points / Second

filtering the shape is getting smoothed. However, it has to be considered that filter techniques as well have an influence on the structure and morphology of the models. These deviations and deformations may lead to varieties of cross sections and could implicate problems for later tree-ring integration. Due to that it is necessary to decide for each particular point cloud, depending on the degree of noise, which filters are reasonable. To avoid problems for the following integration of tree rings, it is necessary to keep the shape as realistic as possible but minimize deviations in volume compared to the actual root volume. In any case, not all outliers can be detected by algorithms available and some erroneous points have to be removed manually. The number of outliers is dependent on the filter technique used. After manually removing parts which belong to other objects (e.g. the fixture) on average 885 outliers out of 86498 points were detected (1.02%). Removing these outliers took about 2–3 min time.

For the ongoing modeling procedure a closed surface representing the body of the scanned object needs to be generated by wrapping the point cloud. The Geomagic software offers two techniques to generate these surface models, a triangulation method and the NURBS (Non Rational b-Splines) technique (Fig. 2) (Terzopoulos and Qin 1994).

Due to the shadowing effect parts of the object can be underrepresented in the point cloud or zones represented by noise need to be removed completely. In these cases interpolation algorithms were applied to fill the resulting holes in the surface model (Fabris et al. 2007). Geomagic provides two main algorithms to fill these holes: one is filling the holes by using a flat layer, the other is curvature based, filling the hole taking into account the curvature of the surrounding areas. The impact of these two interpolation methods on the volume calculations was tested.

For this, different holes were cut artificially into the surface of the root model. The sizes ranged from 1×1 cm to 3×7.5 cm and were placed in regions with a high curvature as well as in regions with a flat structure. Three different filling techniques were used with Geomagic: one automatic (Fig. 3 a, b, e) and two semi-automatic filling techniques (c, d, f). During the two latter techniques a carrying skeleton was manually added and the remaining smaller holes were then filled automatically. The application of hole-filling techniques is case specific. For smaller holes automatic filling was in general sufficient whereas bigger holes and holes with intense curvature of the surrounding needed a semi-automatic approach.

Ring-width data

Discs were cut out of the root perpendicular to the root axis to analyze the annual growth of the root segment. Afterwards the disks are sanded to ensure a plane surface. On each disc, ring widths are measured along four radii according to standard techniques in dendrochronology (Cook and Kairiukstis 1990) using the software WinDENDRO (Regent Inst. 2004). In general radii are positioned perpendicular to each other. However, in some cases it was not possible due to deformations or cracks and angles had to be modified. WinDENDRO enables measuring ring-width variations based on scan images of the polished discs generated by a distortion free flatbed scanner.
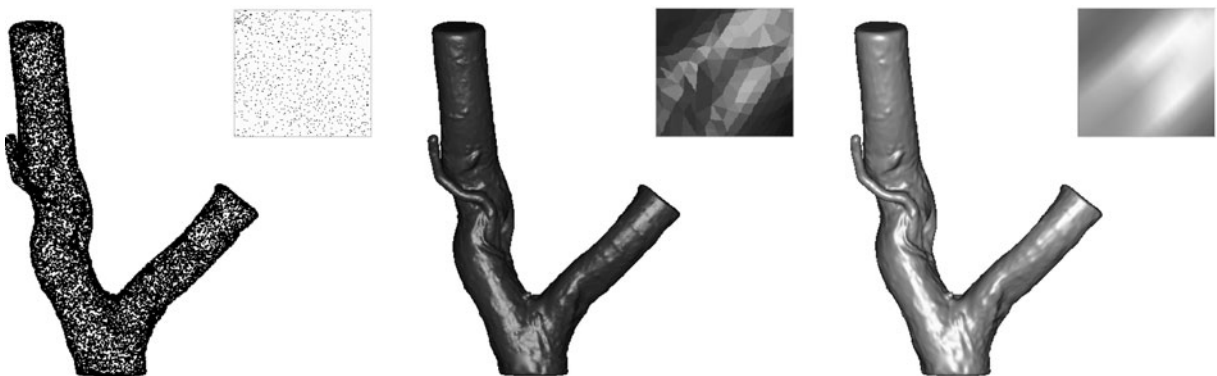

Fig. 2 Point cloud representation of a root segment (left) and resulting surface models based on triangulation (center) and non rational b-splines (NURBS, right)
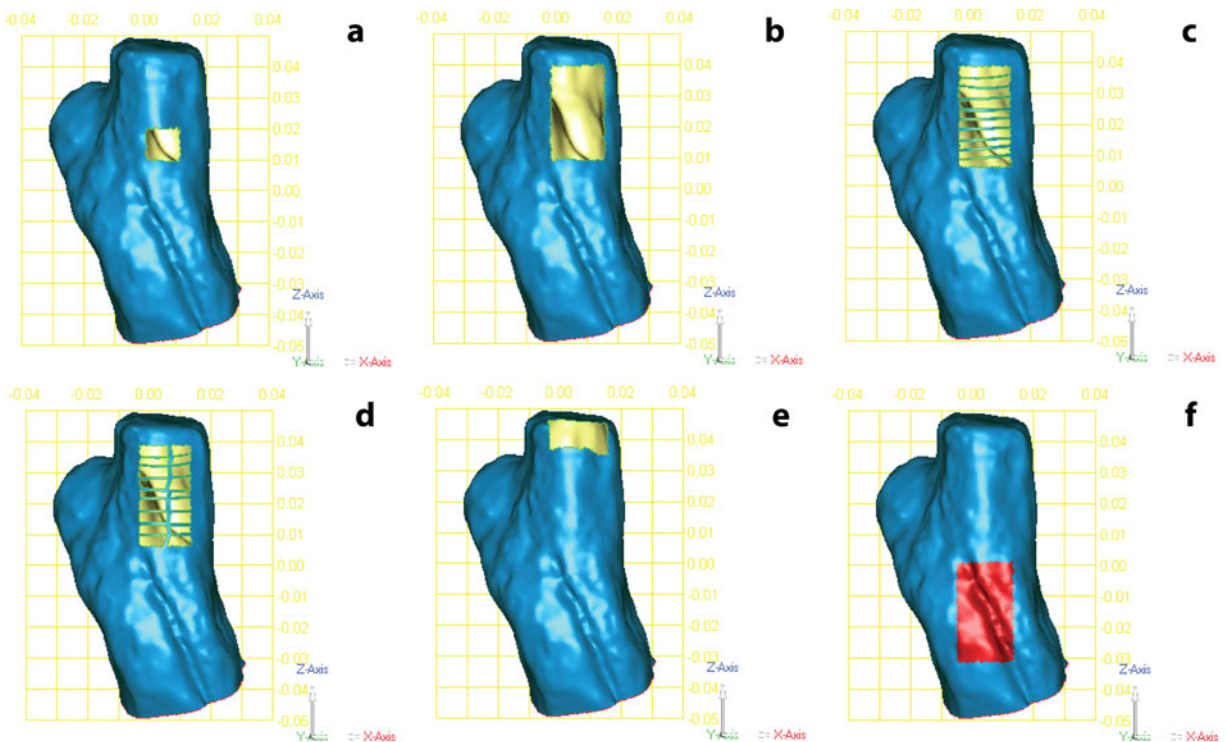
Fig. 3 Automatic (**a**, **b**, **e**) and semi-automatic (**c**, **d**, **f**) hole filling techniques applied to different hole sizes (**a**, **b**, **e**), with different curvature degree (**f**) and carrying skeleton technique (**c**, **d**)

Radii measurements ranging from the outermost ring boundary to the center of the root disc (Fig. 4a). The output data of WinDENDRO are measured distances (ring width) provided as text files and hence, lack of coordinates.

For the following integration of the 2D ring-width data into the 3D model of the root surface, it has to be taken into account that the ring data are representing the wood of the root only, while the surface model also includes bark. Consequently, the thickness of the bark at the outermost point of each radius also needs to be added to the total length of each radius. Finally, distances (s) between the outermost points of the four radii (bark position) are measured additionally since they are essential for later calculations of the correct orientation of the radii (Fig. 4b) within the 3D model.
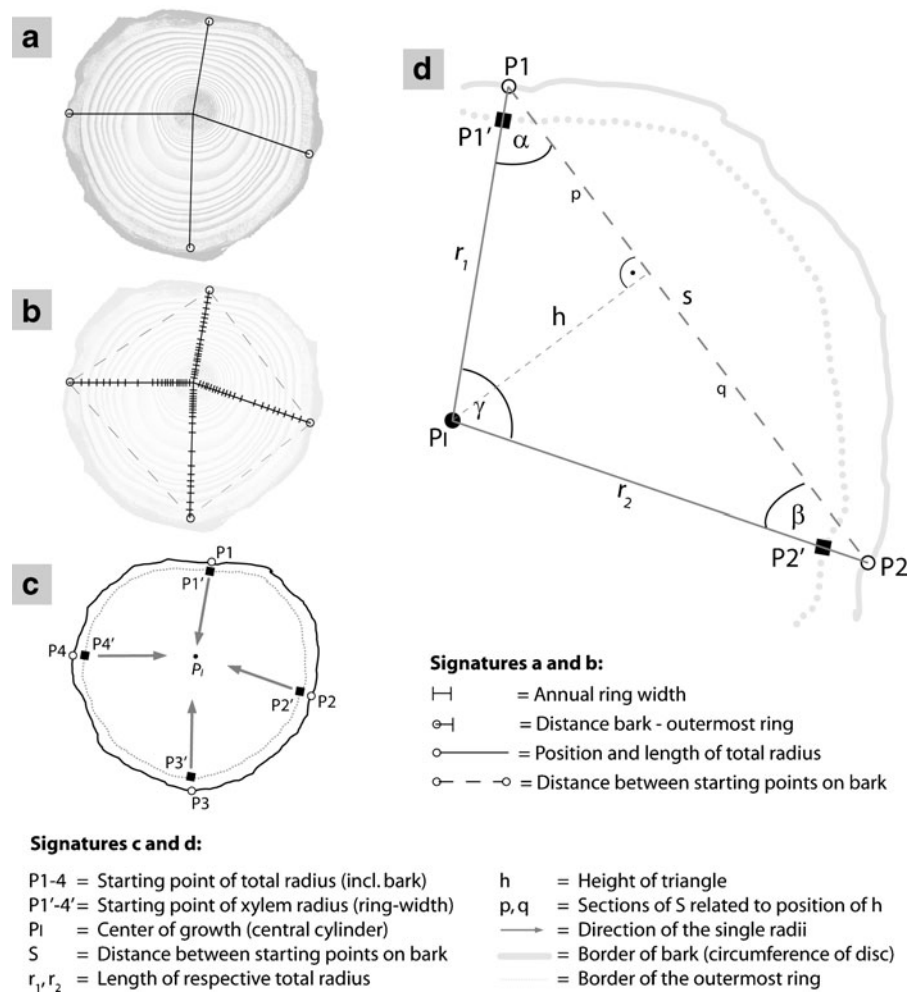
The position of each disc is then determined in the 3D surface model of the root and corresponding cross sections are generated in Geomagic as 2D line segments showing the circumference of the respective disc. We marked the positions of the cross sections with needles before scanning the entire root system, representing later the corresponding reference points (P1); compare Bert and Danjon (2006).

Moreover, it is possible at any time to cut additional cross sections into the model and to extend the amount of input data. The line segments are then converted to a point object. While data points along these cross sections are represented by x/y/z - coordinates, the tree rings are measured in distances and thus lack coordinates. The coordinates of the starting points (P1–P4) of the radii and the single rings (here: position of ring boundaries) need to be calculated to finally combine the 2D ring-width data and the 3D surface model. Trigonometric formulas based on Gruber and Joeckel (2007) need to be defined to determine the correct orientation of the measured radii within the model. However, before such calculations could be accomplished, the z-coordinates of the cross sections were set to be constant in order to conduct calculations in a 2D rather then in a 3D coordinate system.

Results

The radii including the ring-width data measured in WinDENDRO were successfully integrated into the

Fig. 4 (a) Root disc and position of the four radii for the detailed WinDENDRO measurements of (b) ring-width and distance of the radii's starting points; (c) model cross section indicating ideal starting points and directions (*arrows*) of radii and (d) trigonometric parameters to calculate the intersection point P_I and starting points P3-P4 based on real measurements

Signatures a and b:

⊢	= Annual ring width
⊶	= Distance bark - outermost ring
⊙—	= Position and length of total radius
⊙— – –⊙	= Distance between starting points on bark

Signatures c and d:

P1-4 = Starting point of total radius (incl. bark)
P1'-4'= Starting point of xylem radius (ring-width)
P_I = Center of growth (central cylinder)
S = Distance between starting points on bark
r_1, r_2 = Length of respective total radius

h = Height of triangle
p, q = Sections of S related to position of h
⟶ = Direction of the single radii
= Border of bark (circumference of disc)
= Border of the outermost ring

3D model of the root segment by keeping the correct orientation of the single radii relative to each other. The data of the four radii were oriented within the section in order to represent the ring boundaries within the respective cross section of the model. In Geomagic, the position (x/y-coordinates) of the starting point of the first radius including bark (**P1**; Fig. 4c) was determined manually on the point segment representing the cross section. The starting point of the second radius **P2** was then defined by using the segment length **s** measured in WinDEN-DRO, which is the distance between P1 and P2 on the real root disc (Fig. 4c). The intersection of **s** starting in **P1** and the line segment defined the position of **P2**.

The segment **s** and the radii r_1 and r_2 starting in P1 and P2 respectively, form a triangle (Fig. 4d). The intersection of both radii represents the position of the initial growing point (for roots: central cylinder) of the cross section, the intersection point P_I (Fig. 4c, d). The segment **p** and the height (**h**) on **s** were calculated in order to determine the position of P_I (Fig. 4d).

$$\mathbf{p} = \left(s^2 + r_1^2 - r_2^2\right)/2s$$

s   segment length between the starting points of the two radii
r_1 / r_2 length of radius 1 and 2, respectively

$$\mathbf{h} = \pm\sqrt{\left(r_1^2 - p^2\right)}$$

p   segment on s
r_1 length of radius 1

The orientation of the radii (Fig. 4c) was then calculated by using two auxiliary quantities, the transformation constants a and o:

$$\mathbf{a} = (x_2 - x_1)/s$$

$$\mathbf{o} = (y_2 - y_1)/s$$

x_1, y_1 coordinates of P1
x_2, y_2 coordinates of P2
s   segment length between the starting points of the two radii

Finally, based on the formulas described above, the coordinates of the intersection point $\mathbf{P_I}$, determined by the position of the first two radii, were calculated. Because the triangle can be created on both sides of the segment **s**, two results for the intersection point are possible. Obviously, the correct intersection point is always the one lying within the boundaries of the cross section. This fact was integrated as a constraint in the programming procedure. The same calculations were used to calculate P3 and P4, but then $\mathbf{P_I}$ was used as a second input value for these calculations.

$$\mathbf{y_I} = y_1 + o*p + a*h$$

$$\mathbf{x_I} = x_1 + a*p - o*h$$

x_1, y_1 coordinates of P1
h   height on s
p   segment on s

Consequently, the coordinates for the four starting points of radii measurements and the growth origin $\mathbf{P_I}$ as well as the correct orientation of the radii in the coordinate system of the model were known. Finally, the coordinates of the ring boundaries (Rn) along the radii were calculated as follows:

$$\mathbf{y_{Rn}} = y_{PI} + (y_{PX} - y_{PI})*rw/r \tag{1}$$

$$\mathbf{x_{Rn}} = x_{PI} + (x_{PX} - x_{PI})*rw/r \tag{2}$$

Px   Starting point of respective radius (P1, P2, P3, P4)

rw   distance ring boundary to $\mathbf{P_I}$
r   corresponding radii

Based on this, ring-width data (distances) along the radii were transferred into the coordinate system of the corresponding cross section. As a result, every tree ring boundary received its own x, y and constant z coordinate.

As mentioned above, however, the root volume computed using the models showed an offset compared to the actual root volume. This offset also induced a considerable deviation between the shape of the computed cross sections and the corresponding actual shapes. Due to this deviation and the fact that calculations for the integration of the ring-width data were based on the data of the real cross sections, the deformations may result in diverging positions of radii within the cross sections. This could result in the starting points P3 and P4 to be not always directly positioned on the borderline of the cross section (Fig. 5b).

The orientation of the four radii remained consistent to each other building up a radii complex, so that angles between the radii as well as the ring-width data matched the real values measured with WinDENDRO (Figs. 4 and 5a, b). Hence, the entire complex of the 4 radii was reoriented within the cross section of the model to find the correct orientation (Fig. 5c–e).

This optimization problem was solved for the cross sections using a MATLAB program (MathWorks 2008) requiring as input parameters the coordinates of P1–P4, the center point $\mathbf{P_I}$, the single radii and the data points of the cross section.

The program first calculated the distances between the outermost point of each radius to the respectively closest point on the circumference. Afterwards the mean value of the four distances was calculated as well as the standard deviation of distances. This standard deviation was then used to evaluate the optimized configuration of the radii. A configuration was defined by a translation vector (Δx, Δy) and a rotation angle θ of the center of the radii complex ($\mathbf{P_I}$). The values of Δx and Δy were both incremented and decremented stepwise to evaluate different configurations. For each translation step (0.02 mm), the rotation angle was also incremented or decremented stepwise by 5°, but can be reduced case specific. The maximal rotation angle around the center of the radii complex was set ±30°. The circumference of the cross
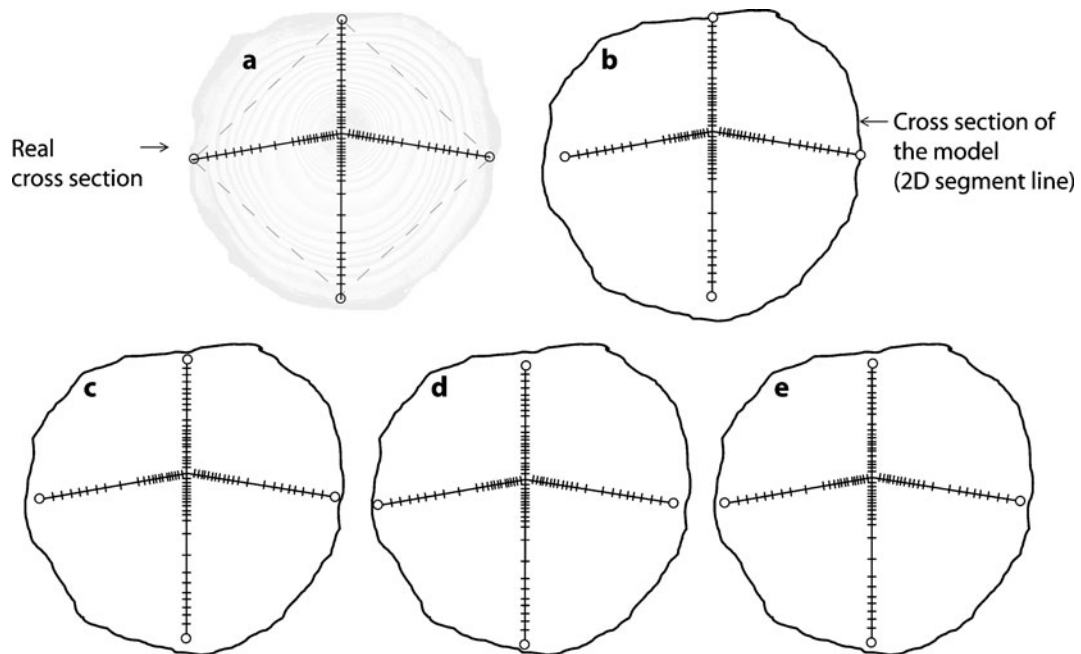
Fig. 5 (**a**) real cross section and position of radii; (**b**) radii integrated into the model cross section based on trigonometric parameters (compare Fig. 5) with two starting points intersecting the segment line; (**c**, **d**) possible, but not optimized positions of the radii within the model section (distance of the four starting points to the borderline unequally distributed); (**e**) optimized position of the radii within the model section (distances equally distributed)

section acted as a constraint for valid configurations. In particular, translation or rotation in a specific direction was stopped as soon as the outermost point of one of the four radii intersected the circumference of the cross section.

Experimental results showed that the optimal configurations were those which minimized the standard deviation of the four distances between the outermost points of the radii and the corresponding intercepts on the circumference of the cross section. For each cross section several configurations were computed and evaluated with MATLAB. Figure 6 exemplifies the development of the standard deviation for two of the cross sections during the rotation and translation phase and the new optimized position based on the smallest standard deviation. Depending on the rotation angle, translation steps and shape of the cross section the number of valid configurations ranged from several hundred up to more than one thousand. The equalized distribution of distances to all four sides compared to the original data set with radii oriented to one side is clearly visible (Fig. 6). The output of the MATLAB script provided the optimal values for the translation steps Δx and Δy and the rotation angle θ based on the smallest value of the standard deviation and finally the optimized coordinates for all data points of the radii complex. The optimized two dimensional cross sections were then imported back to Geomagic which provided a realignment function for objects and transform them back into their original 3D coordinate system (Fig. 7).

Discussion

Compared to the static TLS systems used in former studies (Gärtner et al. 2009; Wagner and Gärtner 2009a), the flexible scan arm used for the recent study reduced the amount of missing data, caused by parts not reached by the laser beam, to a minimum. The rate of improvement in this regard could not be quantified because it strongly depends on the complexity of the structure of the scanned object and the distance between e.g., neighboring roots within the system. As one solution to avoid such shading effects the very dense and complex root systems could be cut in sections and scanned separately (Danjon and Reubens 2008). For the remaining data different interpolation algorithms were tested by Fabris et al. (2007), whose semi-automatic approach showed
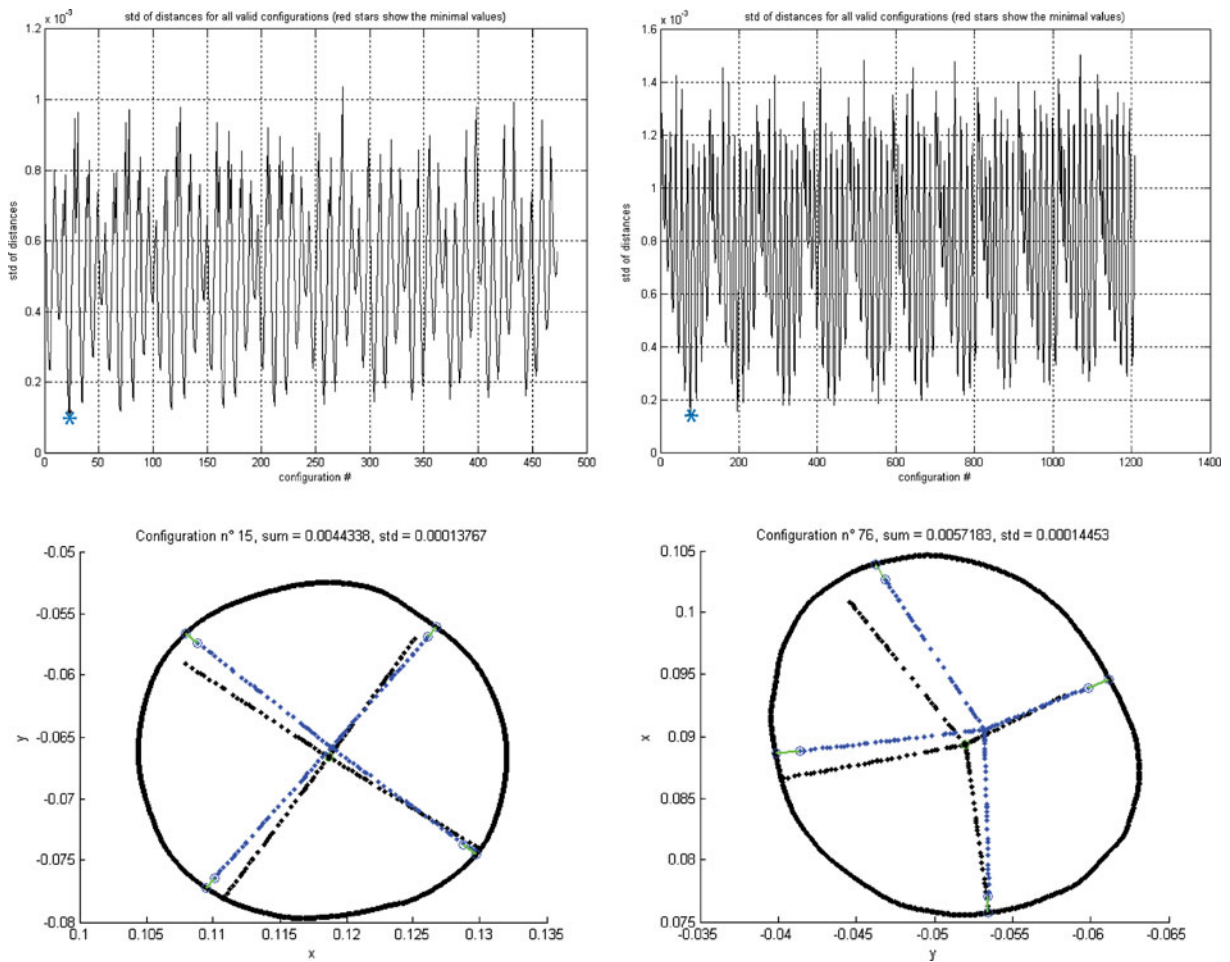
Fig. 6 Automated positioning of radii within the model cross section exemplarily shown for two cross sections. Upper part: Calculated standard deviation for all positions possible (left: 476; right: 1,225) in the respective cross section. Black line = max/min values of all computed constellations; blue star = smallest standard deviation. Lower part: Optimization of respective radii position shown for two cross sections with Matlab. (Black points = calculated radii; blue points: position after optimization according to the lowest standard deviation, blue star above)
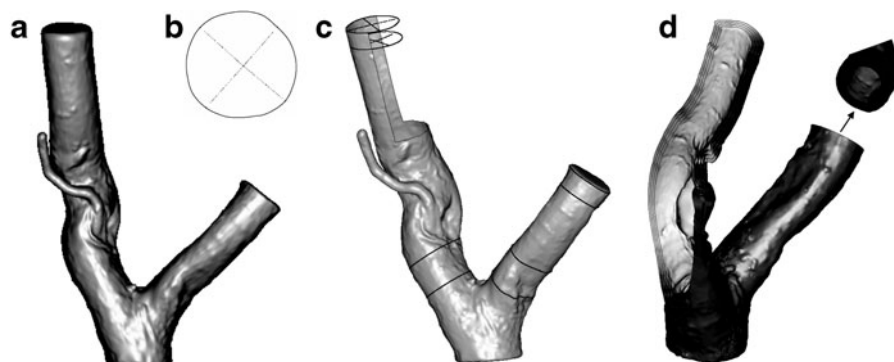

Fig. 7 Approach towards interpolation between the cross sections of the surface model (a); cross section with denoted tree rings (averaged diameter of the cross section: 2.847 cm) (b); cross sections aligned with 3D surface model. (c); nested model of root segments containing different surfaces for age classes (d) as a result of ongoing stepwise interpolation between tree ring radii and cross sections

results comparable to the accuracy of the laser scanner, especially when using carrying skeletons as applied in this study (compare Fig. 3). The point clouds acquired via the scan arm showed, in general, less noise than the point clouds of the TLS, which resulted in a clearly smaller modeling effort (Wagner and Gärtner 2009b). In contrast, the scanning procedure itself was more time consuming. Therefore the registration of single scans was not necessary anymore. However, the scan arm satisfied our expectations and provided an appropriate 3D surface model for following tree-ring integration.

The integration of ring-width data was successful, but an optimization algorithm had to be applied due to deviations and the surface model deviated up to 7% from the original volume. Hence, it is questionable if the ring integration is accurate enough to provide reliable results. In contrast to most photogrammetric devices, LS is not capable of scanning exactly the same point again (Sinderberry 2007). Hence, it needs to be taken into account that the extracted points along the model's cross section used for the integration of annual ring boundaries are always approximations and no absolute values, although the possible offset is in a range of ±0.2 mm only.

Shapes of the cross sections often deviated from those in reality. These variations might be caused by the aforementioned offset in volume or applied filter techniques. Here it is important to mention, that, if a deviation occurs, this always results in a larger volume, compared to the original. This is due to the fact that the penetrating laser beam is not entering the root object but is reflected by its surface and hence, scattering always occurs in the same direction (off the object). In addition, the cross section set in Geomagic might already differ slightly from the position in reality. The growth axis of roots is changing constantly and therefore it is difficult to cut in the exact angle. Besides the system was cut and cross sections were sanded for tree-ring measurements and thus might have caused non-orthogonal cross sections. However, the radii and their orientation to each other is a highly accurate system based on the measurements in WinDENDRO (precise up to 1/100 of a mm) (Regent Instruments Inc. (2004)). It is still questionable, if the offset and deviations of the cross sections are a comprehensive basis for the model developed here.

So far the global carbon cycle is still poorly understood and no accurate biomass models exist

(Heimann and Reichstein 2008), especially no annually-resolved models collecting biomass data on an annual basis. In these terms a new field has been entered. Moreover, many growth models rely just on two cores per tree for the entire tree system. The approach shown in this study is already providing additional information by setting the ring-width data into a spatial context. An optimization algorithm was able to compensate deviations of radii within the cross section. These deformations do not affect the geometry and dimensions of the radii themselves. The orientation of radii remains consistent to each other (angles between radii as well as ring-width data). Moreover, the barks of the roots were included during the scanning procedure which gives a certain tolerance since bark thickness is quite variable.

Even though scanner devices are not yet depicting the object in a ratio of 1:1 it is likely that soon a higher accuracy will be achieved by LS or other related techniques. Furthermore, it needs to be considered that the technique is still new and at least for root-modeling applications the best technique to describe the surface and shape of roots available so far (Danjon and Reubens 2008). No other device used for root studies was able to depicture big root systems in such an accurate way. Hence, laser scanning is an important technique for further coarse-root studies.

Conclusion and perspectives

It was shown that the acquisition of three dimensional structures of exposed coarse root systems was possible by using scan arms. Moreover, it is possible to fully integrate the age information into the model and it will be possible to replace the point clouds from today's scanner generation with the once in future. Due to a high acceptance of laser technique on the market the technical development of laser scanning devices is fast. The companies try to fulfill customer requirements and are developing rapidly new devices and will soon gain higher accuracy and fewer errors (Sternberg 2007). Thus, the effort of integrating the rings into a surface model is fully justified. In fact, the aim is to develop a model which can easily be adapted to the newest stand of technology. Future investigations need to show if this model based on terrestrial laser data is applicable for an entire root system rather then for a root segment and even for

several root systems for comparable root studies. For example if the expenditure of incorporation into software is justifying the model. The biggest expenditure of work is not the data acquisition itself but the post processing of data and the incorporation into software (Brenner 2007).

The basic problem of spatiotemporal modeling of these root systems could be solved by the successful integration of two dimensional ring data into the 3D model of a root segment.

The next step will be to enlarge the approach to integrate the entire ring structure into the model, to interpolate between those cross sections (Fig. 7) and finally, to generate a closed surface for every single year. The implemented radii are essential for ongoing interpolation techniques. Although the calculated volumes from the models based on LS data are diverging from the actual volumes, it is likely that in near future higher accuracy will be achieved and it will be possible to substitute point clouds from the current scanner generation with those from future scanners. Thus, the idea is to create a model, which can always be adapted to the present state of technology and fully justifies the effort of integrating the rings into a surface model. Another important improvement of the model could be to add in future topological information to the 3D model, i.e. define automatically individual roots and branching points, to be able to perform architectural analysis and separate for example sinkers from horizontal surface roots.

References

Aschoff T, Spiecker H (2004) Algorithms for the automatic detection of trees in laser scanner data. ISPRS- Int Arch Photogramm Remote Sens Spat Inf Sci 36:66–70

Bert D, Danjon F (2006) Carbon concentration variations in the roots, stem and crown of mature *Pinus pinaster* (Ait.). Forest Ecol Manag 222:279–295. doi:10.1016/j.foreco.2005.10.030

Bolte A, Rahmann T, Kuhr M, Pogoda P, Murach D, v.Gadow K (2004) Relationships between tree dimension and coarse root biomass in mixed stand of European beech (*Fagus sylvatica* L.) and Norway spruce (*Picea abies* [L.] Karst.).

Plant Soil 264:1–11. doi:10.1023/B:PLSO.0000047777.23344.a3

Brenner C (2007) Interpretation terrestrischer Scandaten. In: DVW e.V. – Gesellschaft für Geodäsie, Geoinformation und Landmanagement (ed) Terrestrisches Laserscanning (TLS 2007). Ein Messverfahren erobert den Raum. Wißner, Augsburg, pp 59–80

Brunner I, Godbold DL (2007) Tree roots in a changing world. J For Res 12:78–82. doi:10.1007/s10310-006-0261-4

Cheng DL, Wang GX, Li T, Tang QL, Gong CM (2007) Relationships among stem, aboveground and total biomass across Chinese forests. J Integr Plant Biol 49:1573–1579. doi:10.1111/j.1774-7909.2007.00576.x

Cook ER, Kairiukstis A (1990) Methods of Dendrochronology—Applications in the environmental science. Kluwer, Dordrecht

Danjon F, Reubens B (2008) Assessing and analyzing 3D architecture of woody root systems, a review of methods and applications in tree and soil stability, resource acquisition and allocation. Plant Soil 303:1–34. doi:10.1007/s11104-007-9470-7

Danjon F, Sinoquet H, Godin C, Colin F, Drexhage M (1999) Characterisation of structural tree root architecture using 3D digitising and AMAPmod software. Plant Soil 211:241–258. doi:10.1023/A:1004680824612

Danjon F, Fourcaud T, Bert D (2005) Root architecture and wind-firmness of mature Pinus pinaster. New Phytol 168:387–400. doi:10.1111/j.1469-8137.2005.01497.x

Drexhage M, Huber F, Colin F (1999) Comparison of radial increment and volume growth in stems and roots of Quercus petraea. Plant Soil 217:101–110. doi:10.1023/A:1004647418616

Fabris M, Achilli V, Bragagnolo D, Menin A, Salemi G (2007) Filling Lacunas in terrestrial laser scanning data: the "Cavallo Ligneo" of the "palazzo della ragione" Padua, Italy. In: "Anticipating the Future of the Cultural Past" CIPA symposium in Athens, 2007. http://cipa.icomos.org/fileadmin/papers/Athens2007/FP059.pdf. Accessed 16 Sep 2009

FARO Technologies Inc. (2009). http://www.faro.com/

Gärtner H (2007) Tree roots-Methodological review and new development in dating and quantifying erosive processes. Geomorphology 86(3–4):243–251

Gärtner H, Bräker OU (2004) Roots—the hidden key players in estimating the potential of Swiss forest to act as carbon sinks. In: Jansma E, Bräuning A, Gärtner H, Schleser G (eds) TRACE—Tree rings in archaeology, climatology and ecology, vol. 2. Jülich, pp 13–18

Gärtner H, Denier C (2006) Application of a 3D Laser scanning device to acquire the structure of whole root systems—a pilot study. In: Heinrich I, Gärtner H, Monbaron M, Schleser G (eds) TRACE—Tree rings in archaeology, climatology and ecology, vol. 4. Jülich, pp 288–294

Gärtner H, Schweingruber FH, Dikau R (2001) Determination of erosion rates by analyzing structural changes in the growth pattern of exposed roots. Dendrochronologia 19:81–91

Gärtner H, Wagner B, Heinrich I, Denier C (2009) 3D laser scanning—a new methodology to analyze coarse tree root systems. For Snow Landsc Res 82:95–106

Geomagic Studio 9.0 and Qualify 9.0 (2007) Available in http://www.geomagic.com/en/products/

Gruber FJ, Joeckel R (2007) Formelsammlung für das Vermessungswesen. Vieweg + Teubner Verlag, Wiesbaden. doi:10.1007/978-3-8351-9106-8_7

Heimann M, Reichstein M (2008) Terrestrial ecosystem carbon dynamics and climate feedbacks. Nature 45:289–292. doi:10.1038/nature06591

Hruska J, Cermak J, Sustek S (1999) Mapping tree root systems with ground-penetrating radar. Tree Physiol 19:125–130. doi:10.1093/treephys/19.2.125

Krause C, Morin H (1999) Root growth and absent rings in mature black spruce and balsam fir, Quebec, Canada. Dendrochronologia 16–17:21–35

Le Goff N, Ottorini JM (2001) Root biomass and biomass increment in a beech (Fagus sylvatica L.) stand in North-East France. Ann Forest Sci 58:1–13. doi:10.1051/forest:2001104

Lichti D, Gordon S, Tipdecho T (2005) Error models and propagation in directly georeferenced terrestrial laser scanner networks. J Surv Eng 131:135–142. doi:10.1061/(ASCE)0733-9453(2005)131:4(135)

Lim K, Treitz PM, Wulder M, St-Onge B, Flood M (2003) LiDAR remote sensing of forest structure. Prog Phys Geogr 27:88–106. doi:10.1191/0309133303pp360ra

Maas HG, Bienert A, Scheller S, Keane E (2008) Automatic forest inventory parameter determination from terrestrial laser scanner data. Int J Remote Sens 29(5):1579–1593. doi:10.1080/0143116070173640

MathWorks Inc (2008) MATLAB Version 7.7.0.471. Available in http://www.mathworks.com

Merk G (2007) Messtechnologie FARO Laser ScanArm. Diploma thesis, ETH Zurich, Switzerland

Nielsen CCN, Hansen JK (2006) Root CSA-root biomass prediction models in six tree species and improvement of models by inclusion of root architectual parameters. Plant Soil 280:339–356. doi:10.1007/s11104-005-3503-x

Pfeifer N, Winterhalder D (2004) Modeling of tree cross sections from terrestrial laser scanning data with free-form curves. Int Arch Photogramm Remote Sens Spat Inf Sci 36:76–81

Regent Instruments Inc. (2004) WinDENDRO: tree ring, stem, wood density analysis and measurement. Quebec City, Canada

Rossmann J, Bücken A (2008) Using 3D-laser-scanners and image-recognition for volume-based single-tree-delineation and-parameterization for 3D-GIS-applications. In: van Oosterom P, Zlatanova S, Penninga F, Fendel EM (eds) Advances in 3D geoinformation systems lecture notes in geoinformation and cartography. Springer, Berlin, pp 131–145. doi:10.1007/978-3-540-72135-2_8

Schulz T (2007) Calibration of a terrestrial laser scanner for engineering geodesy. Dissertation, ETH Zurich, Switzerland/Technical University of Berlin, Germany

Schulz T, Ingensand H (2004) Laserscanning - Genauigkeitsbetrachtungen und Anwendungen. Optische 3D-Messtechnik. Beiträge der Oldenburger 3D-Tage 2004. In: Luhmann Th (ed) Wichmann Verlag, Heidelberg, pp 90–97

Sinderberry M (2007) Accuracy assessment of 3D laser scanning data utilising different registration methods. Faculty of Engineering and Surveying. Bachelor of Spatial Sciences, Queensland, University of Southern Queensland

Sinoquet H, Rivet P (1997) Measurement and visualisation of the architecture of an adult tree based on a three-dimensional digitizing device. Trees 11:265–270. doi:10.1007/s00468 0050084

Sotodeh S (2006) Outlier detection in Laser Scanner Point Clouds. Int Arch Photogramm Remote Sens Spat Inf Sci 36:297–302

Sternberg H (2007) Laserscanning 2007 - die nächste Generation der Systeme. In: DVW e.V. – Gesellschaft für Geodäsie, Geoinformation und Landmanagement (ed) Terrestrisches Laserscanning (TLS 2007). Ein Messverfahren erobert den Raum. Wißner, Augsburg, pp 15–26

Stokes A, Fourcaud T, Hruska J, Cermak J, Nadyezdhina N, Nadyezdhin V, Praus L (2002) An evaluation of different methods to investigate root system architecture of urban trees in situ: I. ground-penetrating radar. J Arboric 28:2–10

Teobaldelli M, Zenone T, Puig AD, Matteucci M, Seufert G, Sequeria V (2007) Structural tree modeling of aboveground and belowground poplar tree using direct and indirect measurements: terrestrial laser scanning, WGROGRA, AMAPmod and JRC_3D Reconstructor. In: P.P.a.H. J (ed) 5th International Workshop on Functional Structural Plant Models. Napier, New Zealand, pp 20-1–20-4. Available at http://algorithmicbotany.org/FSPM07/Individual/20.pdf http://physicsweb.org/articles/news/11/6/16/1. Accessed 20 Januar 2010

Teobaldelli M, Zenone T, Puig AD, Matteucci M, Seufert G, Sequeria V (2008) Building a topological and geometrical model of poplar tree using portable on-ground scanning LIDAR 5th International Workshop on Functional Structural Plant Models, NOV 04–09, 2007 Napier, New Zealand. Funct Plant Biol 35:1080–1090. doi:10.1071/FP08053

Terzopoulos D, Qin H (1994) Dynamic NURBS with geometric constraints for interactive sculpting. ACM T Graphic 13:103–136. doi:10.1145/176579.176580

Wagner B, Gärtner H (2009a) Modeling of tree roots—Combining 3D Laser scans and 2D tree ring data. In: Kaczka R, Malik I, Owczarek P, Gärtner H, Helle G, Heinrich I (eds) TRACE—Tree Rings in Archaeology, Climatology and Ecology, Vol. 7. GFZ Potsdam, Scientific Technical Report STR 09/03, Potsdam, pp 196–204

Wagner, B, Gärtner, H (2009b) 3-D Modeling of tree root systems—a fusion of 3-D Laser scans and 2-D tree-ring data. In: Nell M, Steinkellner S, Vierheilig H, Novak J, Wawrosch C, Franz C, Zitterl-Eglseer K (eds) RootRAP, 7th ISSR symposium Root Research and Applications, Sept 2–4, 2009. BOKU Wien, Institute of Hydraulics and Rural Water Management, Department of Water, Atmosphere and Environment, University of Natural Resources and Applied Life Sciences, Vienna, Austria